Mixed-order transition and tricritical point associated with checkerboard supersolidity in the two-dimensional $t_2 - V_1$ model

Amrita Ghosh,[1,2] Satyaki Kar,[3,4] and Sudhakar Yarlagadda[2]
[1]*Department of Physics, Ben-Gurion University of the Negev, Beer-Sheva 8410501, Israel*
[2]*CMP Division, Saha Institute of Nuclear Physics, HBNI, Kolkata 700064, India*
[3]*Department of Physics, Adamas University, Kolkata 700126, India*
[4]*Department of Physics, Aghorekamini Prakashchandra Mahavidyalaya, Bengai,West Bengal 712611, India*

(Received 11 June 2019; revised manuscript received 15 November 2019; published 28 January 2020)

We use quantum Monte Carlo method employing stochastic-series-expansion technique to study the ground state properties of the $t_2 - V_1$ model of hard-core bosons on a square lattice. We find that, away from half fillings, the minimal combination of nearest-neighbor repulsion V_1 and next-nearest-neighbor hopping t_2 may give rise to checkerboard supersolidity. The nature of the quantum phase transition, where the superfluid changes to a checkerboard supersolid, depends on the relative strength of V_1/t_2 and the average site occupancy. Interestingly, at the half filling, the model displays the extreme Thouless effect. As the filling is varied away from half filling, the model exhibits initially a mixed-order transition, next a tricritical point, and finally a second-order transition.

DOI: 10.1103/PhysRevB.101.035147

I. INTRODUCTION

Ultracold atoms in optical lattices offer a novel platform where generic many-body phenomena of condensed matter physics can be explored [1]. One can study exotic quantum phases such as lattice supersolidity, which is the homogeneous coexistence of superfluidity and crystal order in discrete lattices. In fact, one such example is the recent experimental realization of supersolid phases due to competing short-range and infinite-range interactions for bosonic atoms in optical lattices [2]. The infinite-range interactions are generated by a vacuum mode of the cavity and can be independently manipulated [3,4]. The optical-lattice platform has been quite successful in simulating models for strong correlations such as the Bose-Hubbard models [5] which capture the essential physics of lattice supersolidity as shown by various theoretical works on two-dimensional square lattices [6–15].

Besides the occurrence of lattice supersolidity in artificially engineered optical lattices, a closely-related coexistence of long-range orders [i.e., superconductivity and charge density wave (CDW)] can occur in naturally formed systems. Coexistence of superconductivity and CDW has been observed in a variety of systems such as three-dimensional doped bismuthates [16,17], quasi-two-dimensional doped dichalcogenides [18] and molecular crystals [19], and quasi-one-dimensional doped trichalcogenides [20] and doped spin-ladder systems [21,22].

On the theoretical side, lattice supersolidity has been observed even in simple models such as soft-core-bosons with nearest-neighbor hopping (t_1), nearest-neighbor repulsion (V_1), and on-site repulsion (U) terms in one-dimensional [23] as well as in two-dimensional lattices [11,24]. In the hard-core limit ($U \to \infty$), although the $t_1 - V_1$ model shows the existence of supersolid phase in a triangular lattice [25,26], it fails to display any signature of supersolidity in a square lattice. In an earlier communication [13], it was shown that the $t_1 - t_2 - t_3 - V_1$ model on a square lattice can produce (π, π) (or checkerboard) supersolidity when the same-sublattice tunneling is sizable and nearest-neighbor repulsion is large. In this paper, we study the $t_2 - V_1$ model of hard-core bosons (HCBs) on a square lattice, represented by the Hamiltonian

$$H = -t_2 \sum_{i,j} (d^\dagger_{i+1,j+1} d_{i,j} + d^\dagger_{i-1,j+1} d_{i,j} + \text{H.c.}) + V_1 \sum_{i,j} (n_{i,j} n_{i+1,j} + n_{i,j} n_{i,j+1}), \quad (1)$$

where $d_{i,j}(d^\dagger_{i,j})$ denote the destruction (creation) operator of a HCB at site (i, j), with the number operator being expressed as $n_{i,j} = d^\dagger_{i,j} d_{i,j}$. In Eq. (1), t_2 stands for the next-nearest-neighbor (NNN) hopping amplitude and V_1 signifies the nearest-neighbor (NN) repulsion between the HCBs. In fact, the purpose of the present paper is to demonstrate that the $t_2 - V_1$ model is the minimum model for checkerboard supersolidity in a square lattice with HCBs and to elucidate the rich physics manifested by this model.

The study of $t_2 - V_1$ model dates back to constructing effective Hamiltonians arising due to the presence of cooperative breathing modes observed in oxide systems. Many oxides such as manganites [27], cuprates [28], and bismuthates [29] show evidence of cooperative strong electron-phonon interactions. By including cooperative strong electron-phonon couplings in a Holstein model, an effective Hamiltonian was obtained where the dominant transport comes from double hopping and the dominant repulsion is between nearest neighbors both in one dimension [30,31] and in two dimensions [32].

Phase transitions classified by the Ehrenfest scheme are first order, second order, and higher order. In a first-order transition, the order parameter jumps, whereas its fluctuations

are not large on either side of the transition. Furthermore, coexistence and hysteresis are some of the usual features associated with this transition. On the other hand, a second-order transition is characterized by a lack of discontinuity and anomalously large fluctuations of the order parameter. Contrastingly, Thouless [33] found mixed-order transition indicated by order parameter jumping and displaying large fluctuations. Subsequently, several systems with such mixed-order transition have been reported [34–38]. Interestingly the term "extreme Thouless effect" (i.e., an extreme version of this mixed order), was coined to denote a transition where both the jump and the fluctuations are maximal [39–41]. In this paper, we report another instance of the extreme Thouless effect in the context of the minimum model (i.e., the $t_2 - V_1$ model) for checkerboard supersolidity in a square lattice with HCBs. When the system is below half filling (above half filling), the two-dimensional $t_2 - V_1$ model exhibits either a mixed-order or a continuous transition from a superfluid phase, with particles (holes) equally populating both the sublattices, to a checkerboard supersolid state where all the particles (holes) occupy a single sublattice and hop in it.

The outline of the paper is as follows. In Sec. II, we discuss our numerical techniques and details of the calculations. Section III describes the results obtained and the following discussions. Lastly in Sec. IV, we summarize our work and discuss briefly its novelty. The paper also has an Appendix demonstrating particle-hole symmetry.

II. FORMULATION

To study the various phases of the two-dimensional $t_2 - V_1$ model for HCBs, we employ stochastic-series-expansion (SSE) technique [42,43], a quantum Monte Carlo (QMC) method, involving directed loop updates [44,45]. By identifying $b^{\dagger}_{i,j} = S^{+}_{i,j}$, $b_{i,j} = S^{-}_{i,j}$ and $n_{i,j} = S^{z}_{i,j} + \frac{1}{2}$, to employ SSE, we recast the HCB Hamiltonian in terms of spin-1/2 operators. The converted Hamiltonian, in terms of $2t_2$, takes the form of an extended XXZ Hamiltonian given by

$$H = -\sum_{i,j} \frac{1}{2}(S^{+}_{i+1,j+1}S^{-}_{i,j} + S^{+}_{i-1,j+1}S^{-}_{i,j} + \text{H.c.}) + \sum_{i,j} \Delta_1 \left(S^{z}_{i,j}S^{z}_{i+1,j} + S^{z}_{i,j}S^{z}_{i,j+1}\right) - h\sum_{i,j} S^{z}_{i,j}, \quad (2)$$

with $\Delta_1 = V_1/(2t_2)$. In the above equation we have introduced the term $-h\sum_{i,j} S^{z}_{i,j}$, where h is a variable and can be thought of as a dimensionless external magnetic field acting on the system. By tuning this variable we can access different magnetizations or filling fractions of the system.

In Ref. [31], the one-dimensional $t_2 - V_1$ model was shown to undergo a discontinuous transition from a superfluid phase, with equally populated sublattices, to a checkerboard supersolid state (with homogeneously coexisting CDW and superfluidity), where all the active carriers (i.e., particles below half filling and holes above half filling) are present in a single sublattice. Hence, to study the competition or coexistence of these two diagonal (CDW) and off-diagonal (superfluidity) long-range orders, in the two-dimensional version of the $t_2 - V_1$ model, we use two order parameters: structure factor $S(\vec{Q})$ and superfluid density ρ_s. The structure factor per site is expressed as

$$S(\vec{Q}) = \frac{1}{N_s^2}\sum_{i,j}\sum_{l,m} e^{i\vec{Q}\cdot(\vec{R}_{i,j}-\vec{R}_{l,m})}\langle S^{z}_{i,j}S^{z}_{l,m}\rangle, \quad (3)$$

where $\langle\cdots\rangle$ denote the ensemble average and N_s is the total number of sites of the system. We study $S(\vec{Q})$ at all possible values of wave vector $\vec{Q}$ and identify $\vec{Q} = (\pi, \pi)$ to be the only wave vector for which the structure factor shows peaks. For all other wave vectors $S(\vec{Q})$ remains zero throughout. For $\vec{Q} = (\pi, \pi)$, the structure factor takes the form

$$S(\pi, \pi) = \frac{1}{N_s^2}\sum_{i,j}\sum_{l,m}(-1)^{(i-l)}(-1)^{(j-m)}\langle S^{z}_{i,j}S^{z}_{l,m}\rangle, \quad (4)$$

which, in terms of number operator $n_{i,j}$, can be re-expressed as

$$S(\pi, \pi) = \frac{1}{N_s^2}\sum_{i,j}\sum_{l,m}(-1)^{(i-l)}(-1)^{(j-m)} \times \left\langle \left(n_{i,j} - \frac{1}{2}\right)\left(n_{l,m} - \frac{1}{2}\right)\right\rangle. \quad (5)$$

If for a site (i, j), the sum $(i + j)$ is even then we call it an even site, otherwise it is called an odd site. A square lattice with even number of sites can always be divided into two equal sublattices: even sublattice containing all the even sites and odd sublattices which contains the odd sites. We define the number operators giving the total number of HCBs at even and odd sites as $\hat{N}_e = \sum_{i+j=\text{even}} n_{i,j}$ and $\hat{N}_o = \sum_{i+j=\text{odd}} n_{i,j}$, respectively. Now, the summation in Eq. (5) can be divided into two parts based on the fact that there are two possible scenarios: either both the sites (i, j) and (l, m) belong to the same sublattice or they belong to two different sublattices. Noting that $(-1)^{(i-l)}(-1)^{(j-m)}$ takes the value $+1(-1)$ when (i, j) and (l, m) belong to the same sublattice (two different sublattices), Eq. (5) can be written as

$$S(\pi, \pi) = \frac{1}{N_s^2}\left\langle\left[\hat{N}_e{}^2 + \hat{N}_o{}^2 - \frac{N_s}{2}(\hat{N}_e + \hat{N}_o) + \frac{N_s^2}{8}\right]\right\rangle - \frac{1}{N_s^2}\left\langle\left[2\hat{N}_e\hat{N}_o - \frac{N_s}{2}(\hat{N}_e + \hat{N}_o) + \frac{N_s^2}{8}\right]\right\rangle, \quad (6)$$

which reduces to

$$S(\pi, \pi) = \frac{1}{N_s^2}\langle(\hat{N}_e - \hat{N}_o)^2\rangle. \quad (7)$$

Since the Hamiltonian consists only NNN hopping, both $\hat{N}_e$ and $\hat{N}_o$ commute with the Hamiltonian H; hence we obtain

$$S(\pi, \pi) = \frac{1}{N_s^2}(N_e - N_o)^2, \quad (8)$$

where N_e (N_o) denotes the total number of HCBs at even (odd) sites. Thus, when both the sublattices are equally occupied, i.e., $N_e = N_o$, the structure factor at wave vector (π, π) attains its minimum value, $S(\pi, \pi)_{\text{min}} = 0$. Next, at less than half filling, when all the particles occupy only one sublattice, i.e., either $N_e = N_p$ (N_p being the total number of particles in the system) and $N_o = 0$ or vice-versa, the structure factor

maximizes to

$$S(\pi,\pi)_{\max} = \left(\frac{N_p}{N_s}\right)^2 = \rho^2, \tag{9}$$

where $\rho = \frac{N_p}{N_s}$ is the filling fraction of the system. In terms of magnetization m of the system, this maximum value of the structure factor reduces to

$$S(\pi,\pi)_{\max} = \left(m + \frac{1}{2}\right)^2. \tag{10}$$

On the other hand, as the particle density ρ varies from 1/2 to 1, the maximum value of the structure factor, i.e., $S(\pi,\pi)_{\max}$ reduces to

$$S(\pi,\pi)_{\max} = (1-\rho)^2 = \left(\tfrac{1}{2} - m\right)^2, \tag{11}$$

where $1-\rho$ is the density of holes.

Let us now turn towards the other variable of interest, namely, superfluid density. This is the order parameter for the off-diagonal long-range order; it measures the reluctance of the state (in our case, the ground state) to follow any external phase twist and maintaining persistent, dissipationless flow/hoppings [46]. In a QMC simulation, superfluid density is related to a quantity called winding number that counts the average of cyclic permutations of the identical particles in a single loop update of the worldlines [43]. In terms of winding numbers along x and y directions, W_x and W_y, the superfluid density can be expressed as

$$\rho_s = \frac{1}{2\beta}\langle W_x^2 + W_y^2\rangle, \tag{12}$$

where β denotes the inverse temperature. One can calculate the winding number in the x direction as $W_x = \frac{1}{L_x}(N_x^+ - N_x^-)$, where N_x^+ (N_x^-) represents the total number of operators transporting spin in the positive (negative) x direction with L_x being the length of the lattice along the x direction.

As discussed in Ref. [47], simulating a $L \times L$ square lattice system using SSE method requires a large $\beta \sim L$ in order to capture the ground-state properties of the system. Since our numerical calculations for both $\beta = 3L/2$ and $\beta = 2L$ produce the same results (within the error bars of our calculations), in this paper we consider $\beta = 3L/2$ to describe the ground state results of the system. Now, the SSE QMC calculations also introduce a small parameter ϵ in order to make sure that all the two-spin matrix elements [43] are positive (and thus can be treated as probabilities). In principle, this parameter must be a small positive number and the value of it should not affect the numerical results. However, for large values of anisotropy (i.e., large values of Δ_1 in our case), the autocorrelation time can be substantially affected by the value of ϵ used in the numerical simulation [44]. Therefore, it is important to study the autocorrelation time at various regimes of the phase diagram and make sure that the bin size used in the calculation of the observables is much larger than the autocorrelation time in all the cases. To calculate the autocorrelation time we use the formula

$$\tau_{\text{int}}[m] = \frac{1}{2} + \sum_{t=1}^{\infty} A_m(t), \tag{13}$$

with

$$A_m(t) = \frac{\langle m(i+t)m(i)\rangle - \langle m(i)\rangle^2}{\langle m(i)^2\rangle - \langle m(i)\rangle^2}, \tag{14}$$

where i and t represent the Monte Carlo steps and $\langle\cdots\rangle$ indicates the average over time. We measure the autocorrelation time in the vicinity of the phase transitions, where we expect the autocorrelation times to be larger, as well as far away from them. Since, in the case of two-dimensional $t_2 - V_1$ Hamiltonian, all the phase transitions occur at apparently lower values of anisotropy, we find that we can safely use $\epsilon = \Delta_1/4$, keeping consecutive bins used in the QMC simulation as independent of the other (with bin-size > the autocorrelation times). The bin size we have used for our calculations is 700 000, which is sufficient to keep the autocorrelation times well within the bin size.

III. RESULTS AND DISCUSSIONS

To construct the phase diagram, we study the system at different anisotropy values by varying the magnetization m from -0.5 to 0.5 with $m = \sum_{i,j} S^z_{i,j}/N_s$. In terms of particle filling fraction, this corresponds to the variation of particle density ρ ($= m + 1/2$) from 0 to 1. The particle-hole symmetric Hamiltonian forces the physics for particles at any filling fraction to be identical to the one for holes at the same filling. One should note that, when we vary the particle density ρ from 0 to 1/2 (from 1/2 to 1), the relevant physics should be determined by the particles (holes); the corresponding $S(\pi,\pi)_{\max}$ value is given by Eq. (10) [Eq. (11)].

Figure 1 displays the variation of the superfluid density ρ_s and the structure factor $S(\pi,\pi)$, for four different values of Δ_1, as the magnetization m of the system is tuned from 0 to 0.5; identical results hold when m is tuned from 0 to -0.5 as demonstrated through the calculations displayed selectively by Figs. 8 and 9 in Appendix. Although Appendix contains figures corresponding to $\Delta_1 = 1.214$ and $\Delta_1 = 1.22$ only, similar results also hold true for $\Delta_1 = 1.10$ and $\Delta_1 = 1.50$ considered in Fig. 1. Hence, within the error bars of our calculations, m can be regarded as absolute value of the magnetization $|m|$ in Fig. 1. *We will interpret our results for particle-density ρ variation between 0 to 1/2 corresponding to m being tuned from -0.5 to 0.* For a small value of NN anisotropy, $\Delta_1 = 1.10$ [as in Fig. 1(a) and its equivalent for $m \leqslant 0$], the system manifests superfluidity over the whole range of magnetization, where both the sublattices are equally occupied by the particles, giving rise to a zero structure factor. At a slightly higher value of $\Delta_1 = 1.214$ [see Figs. 1(b) and 8], we find superfluid (SF) density to undergo a downward kink at around $m \approx -0.26$. Beyond this point, a $S(\pi,\pi)$ order develops in the system which continuously increases to soon mimic the $S(\pi,\pi)_{\max}$ curve, as given by Eq. (10) (accompanied by a continuous decrease in the superfluid density). The system undergoes a continuous transition from a SF to a checkerboard supersolid (cSS) phase with both the $S(\pi,\pi)$ order and superfluidity coexisting homogeneously. As soon as $S(\pi,\pi)$ becomes equal to $S(\pi,\pi)_{\max}$, we get all the particles occupying a single sublattice in the ground state. As we further go to higher values of Δ_1, surprisingly the nature of the phase transition changes. For example, for

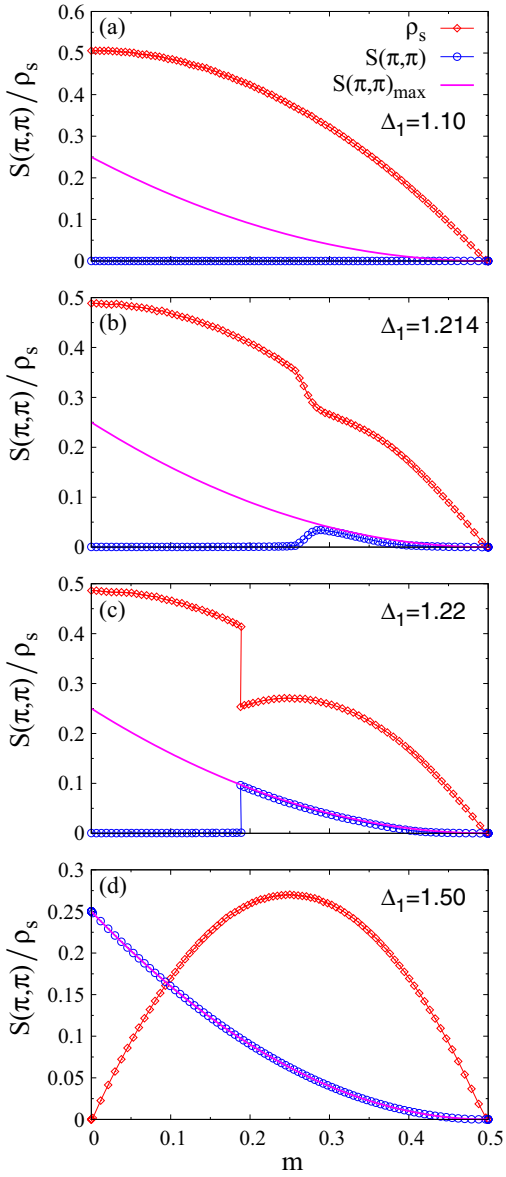

FIG. 1. Plots of superfluid fraction ρ_s and structure factor $S(\pi,\pi)$ on a 32×32 lattice for four different values of anisotropy: (a) $\Delta_1 = 1.10$, (b) $\Delta_1 = 1.214$, (c) $\Delta_1 = 1.22$, and (d) $\Delta_1 = 1.50$. The magenta solid line represents the maximum value of the structure factor, i.e., $S(\pi,\pi)_{\max}$, when all the holes occupy the same sublattice. Similar results hold for $0 \leqslant -m \leqslant 0.5$ and hence m can be regarded as absolute value of magnetization $|m|$ in the above plots. For $0 \leqslant -m \leqslant 0.5$, results similar to (b) are depicted in Fig. 8 and plot similar to (c) is displayed in Fig. 9.

$\Delta_1 = 1.22$ one can see from Figs. 1(c) and 9 that initially the system manifests a SF phase, but around $m \approx -0.188$ the system undergoes striking jumps in order parameters, similar to a first-order phase transition from a SF phase to a cSS phase, pushing all the particles to occupy a single sublattice. On the other hand, similar to a second-order transition, there is a large fluctuation in the particle number in a sublattice. In fact, at the transition there is a large degeneracy (i.e., equal to approximately the total number of particles) and the entropy shoots up. The degenerate states at this *strange*

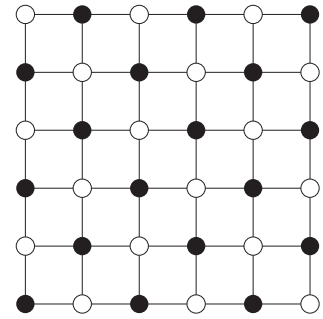

FIG. 2. Checkerboard solid, realized at half filling for large repulsion values, for which the structure factor $S(\pi,\pi)$ produces the maximum peak. The black circles denote particles, whereas the empty circles stand for holes.

phase transition can have single-sublattice occupancy ranging from zero particles to the total number of particles; thus, the fluctuations of single-sublattice occupancy is spread all over the permitted range of variation of the parameter. This transition is the exotic extreme Thouless effect [39,40]. In the context of the one-dimensional $t_2 - V_1$ model dealt with in Ref. [31], a similar extreme Thouless effect was detected as can be seen from Figs. 1, 4, and 5 of that work.

At even higher Δ_1 values, such as $\Delta_1 = 1.50$, the particles/holes form a checkerboard solid (cS) at half filling (i.e., $m = 0$) with $S(\pi,\pi) = S(\pi,\pi)_{\max}$, where one sublattice is completely filled and the other one is completely empty. For any value of repulsion Δ_1, we are interested only in the minimum-energy state. Thus, when $\Delta_1 = 0$, the ground state corresponds to both the sublattices being equally occupied as this is the lowest-energy state based on kinetic energy and we get a superfluid. Next, for nonzero values of the repulsion, at some critical value of Δ_1, in the ground state at half filling, the particles arrange themselves on alternate sites (as depicted in Fig. 2) to avoid the nearest-neighbor repulsion and we get a checkerboard solid. In the ground state below half filling, superfluidity develops and the system exhibits a cSS order which continues all the way to $m = -0.5$. Now, based on the competition between the hopping and the repulsion term in the Hamiltonian, one can explain Fig. 1 and Figs. 8 and 9. It is important to note that, to minimize the energy, larger NN repulsion V_1 favors the formation of checkerboard order by restricting the particles to be in a single sublattice, whereas the NNN hopping t_2 favors equal occupation of both the sublattices. In the case of Fig. 1(a) and its equivalent for $m \leqslant 0$, the NN repulsion is not large enough to restrict the particles in one sublattice; instead, it is energetically favorable for the system if the particles are equally distributed in both sublattices and they hop to different sites thereby lowering their energy and giving rise to superfluidity for all filling fractions. On the other hand, for large repulsion values, such as $\Delta_1 = 1.50$ in Fig. 1(d) and its equivalent for $m \leqslant 0$, at half filling the particles/holes arrange themselves in alternate sites to avoid NN occupation and thus form a checkerboard solid as depicted in Fig. 2. Next, if one considers the case where we dope the half-filled system with holes, the relevant physics should be described in terms of particles. In this scenario, above a critical repulsion Δ_1, all the particles occupy one

sublattice which is partially filled because the system is below half filling. This resembles the situation of a partially-filled band involving one sublattice. Now, by the virtue of NNN hopping t_2, the particles can hop to NNN sites (preserving a checkerboard CDW state due to single sublattice occupancy of particles) and thus lower the energy. This results in the homogeneous co-existence of superfluidity and CDW, i.e., a checkerboard supersolid phase, where each and every particle of the system participates in the CDW formation as well as superfluidity. This cSS phase persists all the way up to filling fraction 0. Similarly, if one considers the case where we dope the half-filled system with particles (i.e., the case where the system is above half filling), the physics should now be described in terms of holes. In this scenario, above a critical repulsion Δ_1, all the holes will occupy one sublattice which is partially filled. Therefore there are some NNN sites (in the same sublattice) available for the holes to hop by virtue of NNN hopping. As a result we have a supersolid phase for holes where the holes can hop in the same sublattice still maintaining a CDW structure in the background; each and every hole participates in the CDW state as well as superfluidity.

Now, for the intermediate values of repulsion, such as $\Delta_1 = 1.214$ and $\Delta_1 = 1.22$ in Figs. 1(b) and 1(c) or Figs. 8 and 9, the repulsion is not strong enough to form a cS at half filling. Since there is a substantial amount of particles present in the system (for filling fraction $1/2$ and in its vicinity), initially it is energetically favorable for the system to be in the superfluid phase, where the particles can lower their energy by hopping to other sites. In this phase (where both sublattices are equally occupied by particles), although the particles experience NN repulsion, the energy lowered by the hopping process is large enough to overcome this energy cost. Single sublattice occupancy or two sublattice occupancy is determined by energy consideration only.

The results shown in Fig. 1 and Figs. 8 and 9 imply that, in between $\Delta_1 = 1.214$ and $\Delta_1 = 1.22$, the system must have passed through a tricritical point at which the nature of the phase transition (between SF and cSS) changes from continuous to mixed order. To locate the tricritical point, in Fig. 3, we plot the structure factor $S(\pi, \pi)$ as a function of magnetization m for a number of Δ_1 values. A similar depiction also holds for $0 \leqslant -m \leqslant 0.5$ and hence in Fig. 3 m should be treated a $|m|$. Let us here describe only the results from the 32×32 lattice for $0 \leqslant \rho \leqslant 0.5$. We observe that for $\Delta_1 = 1.17$ the system manifests superfluid phase only. As we increase the NN repulsion, the system passes through a continuous phase transition from SF to cSS. For lower values of Δ_1, the system never reaches a state where all the particles occupy a single sublattice, but as the Δ_1 value goes up the system gets closer to the single sublattice occupancy state. For some NN anisotropy between $\Delta_1 = 1.216$ and $\Delta_1 = 1.217$, the nature of the phase transition changes from continuous to mixed order, which corresponds to a tricritical point. Up to $\Delta_1 = 1.2205$ the system passes through a mixed-order transition from SF to cSS. As the value of Δ_1 is further increased, at $\Delta_1 = 1.221$ the half-filled system manifests a cS phase and goes into a cSS phase in a continuous manner as the density is varied. Although the value of $S(\pi, \pi)$ agrees with the maximum possible value of structure factor $S(\pi, \pi)_{\max}$ for densities close to half filling, it starts to deviate from the

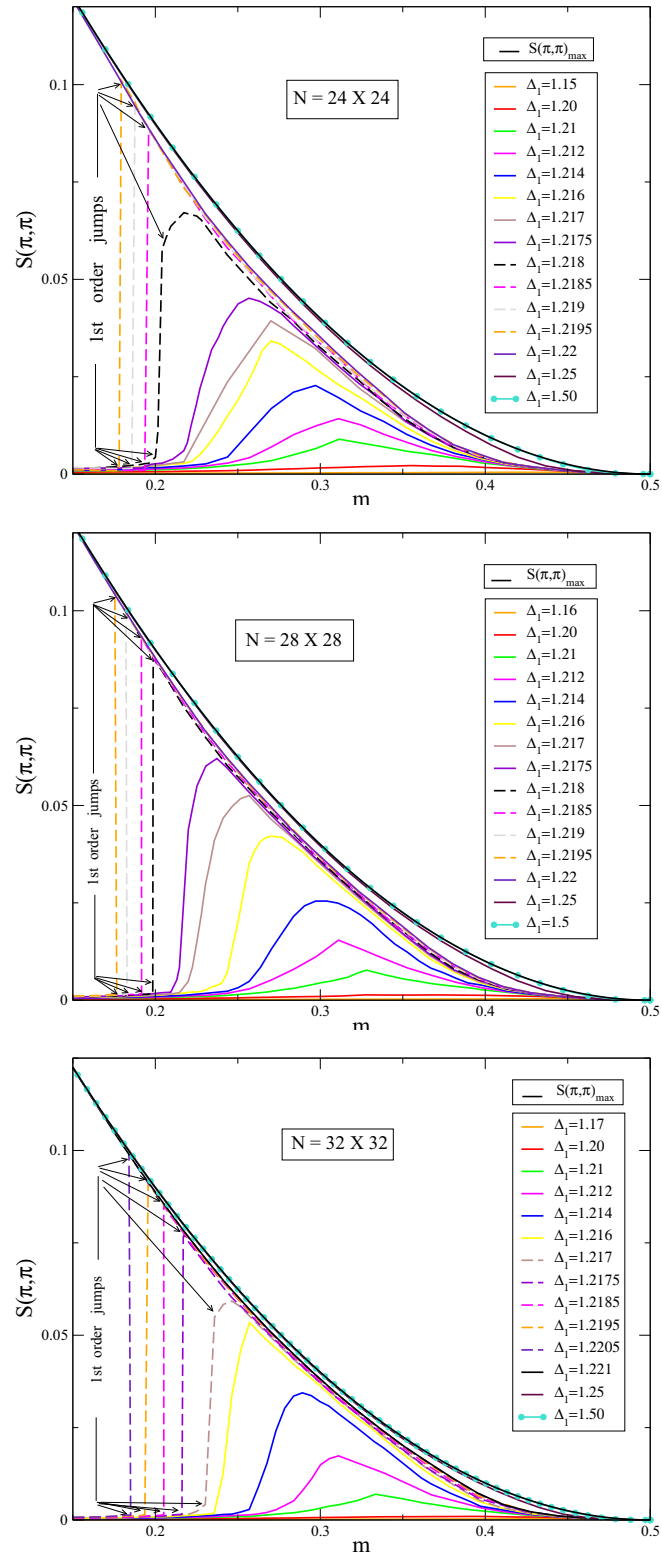

FIG. 3. Plots of structure factor $S(\pi, \pi)$ as the magnetization of the system is varied for different values of NN anisotropy Δ_1. The results are obtained for 24^2, 28^2, and 32^2 size systems, respectively. Similar results hold for $0 \leqslant -m \leqslant 0.5$ and hence m can be regarded as $|m|$ in the above plots.

$S(\pi, \pi)_{\max}$ curve as we go towards the fully-empty system indicating a deviation from the single sublattice occupancy

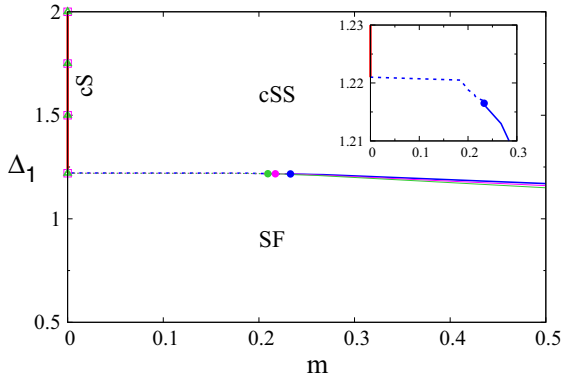

FIG. 4. Phase diagram in terms of magnetization m for HCBs on 24×24, 28×28, and 32×32 square lattice. The green, magenta, and blue dashed (solid) lines represent discontinuous (continuous) superfluid-checkerboard supersolid (SF-cSS) phase transitions as a function of m for 24×24, 28×28, and 32×32 systems, respectively. The three filled circles (green, magenta, and blue) denote the tricritical points for the three different system sizes. The solid red line represents the checkerboard solid (cS) for 32×32 lattice, whereas the magenta squares and green triangles denote the same for 28×28 and 24×24 lattices, respectively. The inset shows phase diagram for 32^2 size lattice zoomed around the tricritical point. A similar result holds for $0 \leqslant -m \leqslant 0.5$ and hence m can be treated as $|m|$.

state. For even larger values of Δ_1 the particles always occupy a single sublattice for all filling fractions and thus the $S(\pi, \pi)$ and $S(\pi, \pi)_{\max}$ curves merge together. It should be noted that in Fig. 3, for the system sizes considered, we have restricted the magnetization axis from 0.15 to 0.5 only because this is the window where the phase transition takes place. For magnetization values between $m = 0$ and $|m| = 0.15$, the structure factor $S(\pi, \pi)$ is essentially zero for all anisotropy values up to $\Delta_1 = 1.2205$, whereas it matches with the theoretical $S(\pi, \pi)_{\max}$ curve for $\Delta_1 = 1.221$ and above.

Figure 3 displays the variation of the structure factor $S(\pi, \pi)$ for different values of Δ_1 and as a function of magnetization measured on 24×24, 28×28, and 32×32 size systems, respectively. Comparing these results one can find that as we increase the system size the number of mixed-order lines increases. For a smaller system size one has to go for smaller repulsion window to identify the tricritical point which makes it harder to detect.

The complete ground-state phase diagram is displayed in Fig. 4 for HCBs on 24×24, 28×28, and 32×32 square lattices. In the phase diagram, the dashed (solid) line represents a discontinuous (continuous) transition from superfluid (SF) to checkerboard supersolid (cSS) region as the magnetization of the system is varied, where the filled circles denote the tricritical points. Note that the three different colors, i.e., blue, magenta, and green, represent the phase boundaries for the three different system sizes 32×32, 28×28, and 24×24, respectively. Apart from the slight shift of the tricritical point, the phase diagram appears to be by and large independent of the system size. We now discuss the phase diagram for the 32×32 square lattice. For anisotropy values $\Delta_1 \leqslant 1.17$, the system manifests superfluidity for all values of magnetization. Beyond this point (i.e., $\Delta_1 = 1.17$) a small region of cSS phase starts to develop, through continuous phase transition, close to $|m| \approx 0.5$. As we increase the Δ_1 value, the magnetization value at which the system goes into the cSS region shifts towards $m = 0$.

In the region between $\Delta_1 = 1.216$ and $\Delta_1 = 1.217$, which is represented as the filled blue circle in Fig. 4, the nature of the transition changes from continuous to mixed order, thereby giving rise to a tricritical point. We observe that for $\Delta_1 \geqslant 1.221$, the system manifests a checkerboard solid (cS) at half filling and beyond $m = 0$ a cSS region, persisting all

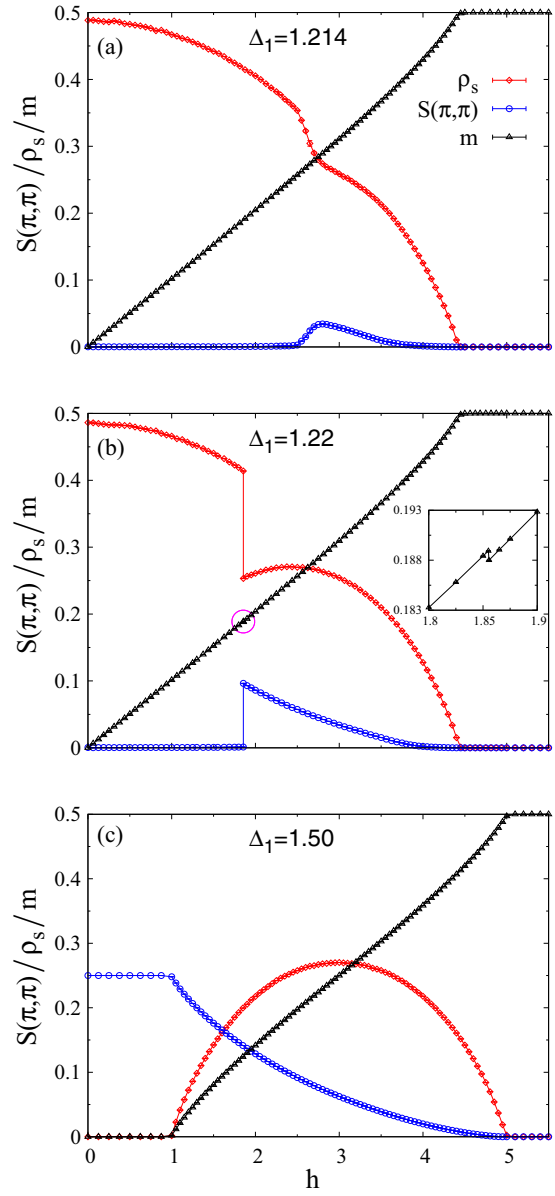

FIG. 5. Evolution of the order parameters $S(\pi, \pi)$, ρ_s, and m as a function of the magnetic field h, on a 32×32 lattice, for three values of anisotropy: (a)$\Delta_1 = 1.214$, (b)$\Delta_1 = 1.22$, and (c)$\Delta_1 = 1.50$. The inset in Fig. 5(b) represents the magnified version of the region encircled by the magenta line. Similar results hold for $h \leqslant 0$ and hence h can be treated as absolute value of magnetic field $|h|$ in the above plots. For $h \leqslant 0$, results similar to (a) are depicted in Fig. 10 and plot similar to (b) is displayed in Fig. 11.

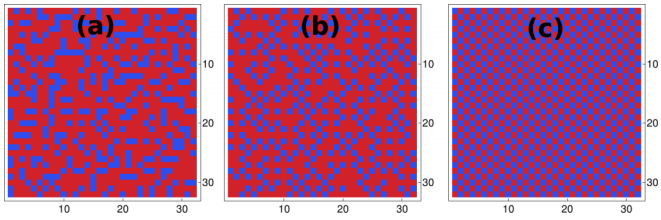

FIG. 6. The snapshot of spin configurations (a) just before and (b) just after the jump as seen in Fig. 5(b) or Fig. 11; and (c) for the case with complete checkerboard order corresponding to Fig. 5(c).The contrasting colors are for opposite spins.

the way to $|m| = 0.5$, is developed. Figures 6(a) and 6(b) show the snapshots of the spin configurations barely before and after the discontinuous jump seen in the ground state corresponding to Fig. 5(b) or Fig. 11. We can clearly see building of checkerboard order (i.e., occupancy along NNN sites or in a single sublattice) beyond this jump. Figure 6(c) also shows a configuration [corresponding to $m = 0$ in Fig. 5(c)] with full checkerboard order where we obtain $S(\pi, \pi) = S(\pi, \pi)_{\max}$.

Now, we want to study the nature of the phase transitions as we vary the magnetization of the system for a fixed value of NN anisotropy. As already seen in Figs. 1(b) and 8, the order parameters show a continuous variation as a function of the magnetization for $\Delta_1 = 1.214$ which signifies continuous phase transition between different phases. On the other hand, the discontinuous jumps in the order parameters in Figs. 1(c) and 9 for $\Delta_1 = 1.22$, indicates the existence of a mixed-order phase transition. However, to bring out the nature of the phase transitions along the m axis of the phase diagram, a more reliable process is to study the order parameters, i.e., magnetization, superfluid density, and structure factor, as a function of the magnetic field h. Figure 5 displays order parameters $S(\pi, \pi)$, ρ_s, and m as a function of the magnetic field h for $h \geqslant 0$; within the error bars of our calculations, similar results also hold true for $h \leqslant 0$. Hence, in Fig. 5, h can be regarded as absolute value of magnetic field $|h|$. Figures 5(a) and 10 show that as we vary the magnetic field h, keeping the NN anisotropy value fixed at $\Delta_1 = 1.214$, the order parameters change in a continuous fashion. This evidently rules out the possibility of a first-order or mixed-order phase transition and establishes the fact that at $\Delta_1 = 1.214$, as we move along the m axis of the phase diagram, the superfluid (SF) and the checkerboard supersolid (cSS) phases are separated by a continuous phase transition. At a higher value of NN anisotropy, $\Delta_1 = 1.22$, a discontinuous jump in the structure factor accompanied by a sudden drop in the superfluid density is observed as a function of the magnetic filed h [see Fig. 5(b) and Fig. 11]; however, there seems to be no visible jump associated with the magnetization curve. Now, zooming into the $m - h$ curve in the region, where the discontinuous jumps in $S(\pi, \pi)$ and ρ_s are observed, we see that the magnetization curve shows a very small but sharp drop as the magnetic field is varied. Usually, whenever a first-order phase transition is encountered by the variation of the magnetic field, a sudden upward jump in the magnetization curve is observed which signifies the existence of a phase-separated region. In contrast to the usual scenario, the mixed-order phase transition, encountered in the case of $\Delta_1 = 1.22$, is not associated with any

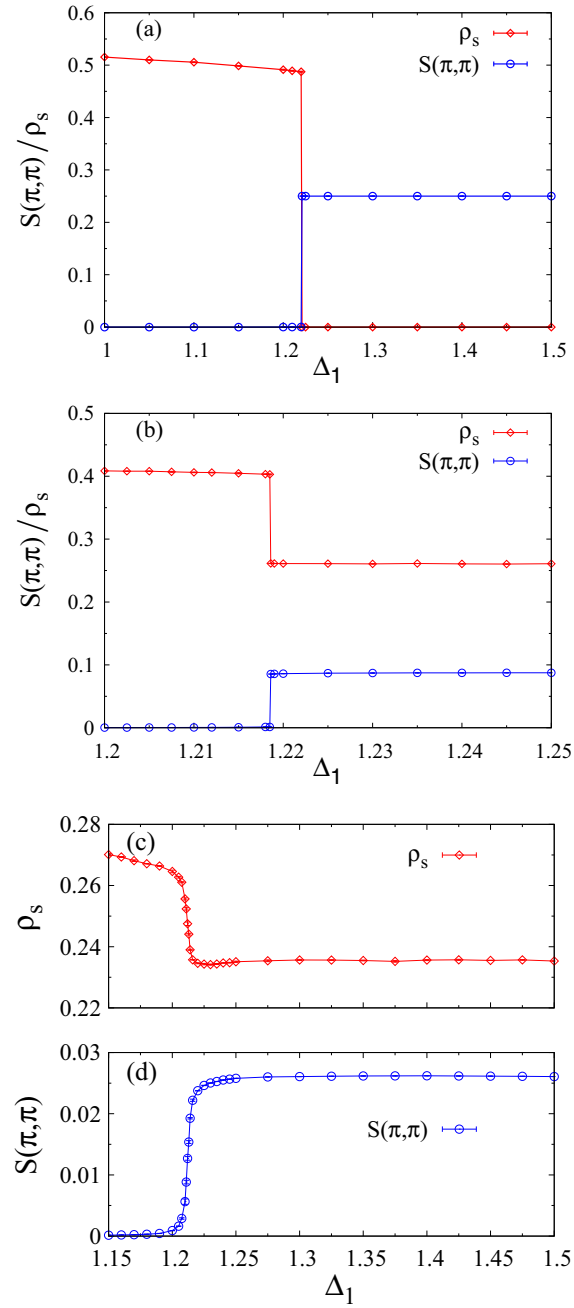

FIG. 7. Plots of $S(\pi, \pi)$ and ρ_s as a function of the NN anisotropy Δ_1 on a 32×32 lattice (a) at half filling (which corresponds to magnetization value $m = 0$), (b) for $m = 0.20404 \pm 0.00001$, and (c),(d) for $m = 0.33840 \pm 0.00003$. Results similar to (b) hold at $m \approx -0.20404$ and figures similar to (c),(d) hold at $m \approx -0.33840$.

phase-separated region. The sharp drop in the magnetization curve simply indicates a mixed-order transition from a superfluid phase with equal sublattice occupancy to a checkerboard supersolid phase where only one sublattice is occupied. Next, for $\Delta_1 = 1.50$, Fig. 5(c) depicts continuous variations of the order parameters as the magnetization of the system is tuned. This means that in the phase diagram shown in Fig. 4, as we move along the m axis keeping value of NN anisotropy fixed at $\Delta_1 = 1.50$, a continuous phase transition, from a

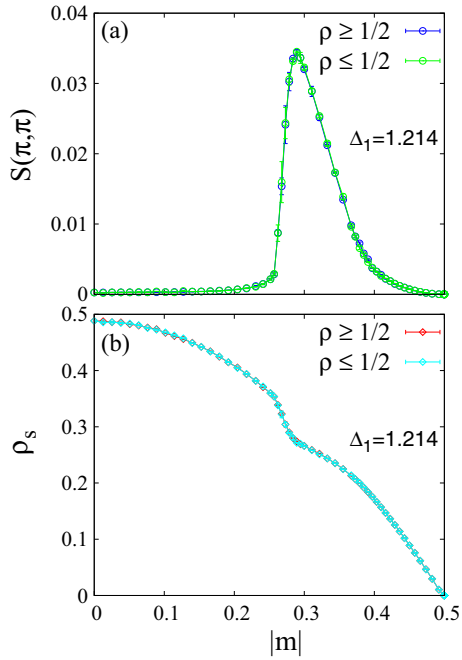

FIG. 8. For the cases of above and below half filling, comparison of the order parameters $S(\pi,\pi)$ and ρ_s as a function of the absolute value of magnetization $|m|$, on a 32×32 lattice, for value of anisotropy $\Delta_1 = 1.214$. Magnetization $m \geqslant 0$ ($m \leqslant 0$) corresponds to $\rho \geqslant 1/2$ ($\rho \leqslant 1/2$).

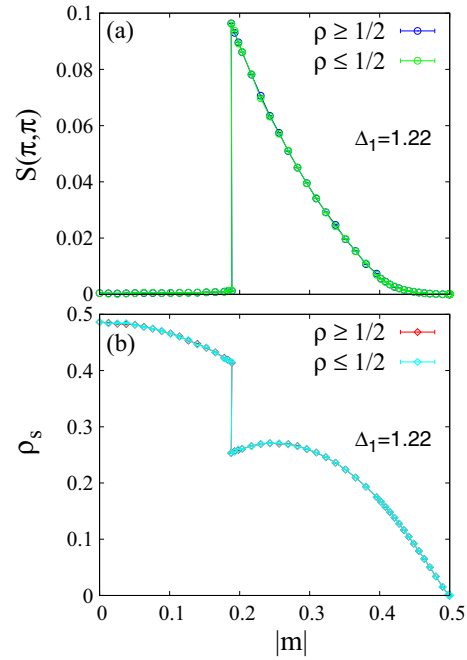

FIG. 9. For the cases of above and below half filling, comparison of the order parameters $S(\pi,\pi)$ and ρ_s as a function of the magnetization $|m|$, on a 32×32 lattice, for anisotropy $\Delta_1 = 1.22$. Magnetization $m \geqslant 0$ ($m \leqslant 0$) corresponds to $\rho \geqslant 1/2$ ($\rho \leqslant 1/2$).

checkerboard solid (cS) to a checkerboard supersolid (cSS) phase, is encountered. The following subsection gives some detailed analysis of the various transitions encountered in the present system.

A. Nature of transitions

To study the nature of the phase transitions encountered while moving along the Δ_1 axis of the phase diagram at a fixed value of magnetization, first it should be noted that, in our simulations, we cannot tune the magnetization of the system directly. Instead, we introduce a magnetic field in the system, by tuning which we can access different magnetization values of the system. Since the resulting magnetization for a particular value of magnetic field generally fluctuates during the simulation, it becomes almost impossible to study the nature of the phase transition by varying the Δ_1 value at a fixed value of magnetization. Nevertheless, while in a charge-density-wave (CDW) state the system always shows plateau in the $m - h$ curve, i.e., the magnetization of the system remains unchanged over a range of magnetic field values. Therefore, we can choose any magnetic field lying in the plateau and obtain the desired magnetization value for different values of NN anisotropy.

Figure 7(a) shows that, at 1/2 filling (corresponding to $m = 0$), as the NN anisotropy Δ_1 is varied from 1.0 to 1.5, the structure factor $S(\pi,\pi)$ sharply jumps from 0 to its maximum value 0.25 at $\Delta_1 \approx 1.221$. At the same time the superfluid density ρ_s dramatically drops down to zero. In the phase diagram depicted in Fig. 4, as we move along the Δ_1 axis at $m = 0$, this indicates a mixed-order phase transition from a $U(1)$ symmetry breaking superfluid (SF) to a translational symmetry breaking checkerboard solid (cS) state at $\Delta_1 \approx 1.221$. It is important to point out that only when the system is in the CDW state after the phase transition, the magnetization can be fixed at $m = 0$; but before the transition, in the superfluid phase, the magnetization is given by $m = 0 \pm 0.00000063$.

As we have already discussed, the dashed (solid) line in the phase diagram in Fig. 4 signifies a mixed-order (continuous) transition between the superfluid and checkerboard supersolid phase. Since the nature of the transition between any two phases should be independent of the driving parameters (Δ_1 or m in this case), irrespective of whether we cross the dashed (solid) line horizontally (by varying the magnetization at a fixed Δ_1 value) or vertically (i.e., moving along the Δ_1 axis at a fixed magnetization value) in the phase diagram, the nature of the transition should remain mixed order (continuous). To demonstrate this point, we concentrate on the phase diagram for the 32×32 square lattice around $|m| \approx 0.204$ and observe that as the Δ_1 value is increased from 1.20 to 1.25, the system goes through a phase transition from SF to cSS. To determine the nature of this phase transition, we vary the magnetic field in very small steps so that we can obtain the magnetization $|m|$ as close as possible to 0.204 for a number of Δ_1 values between 1.20 and 1.25. Figure 7(b) depicts the variation of $S(\pi,\pi)$ and ρ_s in terms of Δ_1 at magnetization $m = 0.20404 \pm 0.00001$. The sharp jumps in the order parameters clearly indicate that in the phase diagram, as we move along the Δ_1 axis keeping the magnetization fixed at $|m| \approx 0.204$, the phase transition, encountered between the superfluid (SF) and checkerboard supersolid (cSS) phase, is mixed order in nature.

Next, in order to determine the nature of the SF-cSS transition while crossing the solid line vertically in the phase diagram of a 32×32 lattice, we plot, in Figs. 7(c) and 7(d), the order parameters $S(\pi, \pi)$ and ρ_s as a function of Δ_1 while keeping the magnetization fixed at $m = 0.33840 \pm 0.00003$. The continuous variation of the order parameters, for $|m| \approx 0.33840$, rules out the possibility of a mixed-order transition. This establishes the point that, irrespective of whether we cross the solid line horizontally or vertically, the nature of the SF-cSS transition remains the same, i.e., continuous.

B. Equivalent models

We will now discuss models that are equivalent to our $t_2 - V_1$ model. As shown by Eq. (2), our model can be mapped onto an extremely anisotropic Heisenberg model (with nearest-neighbor Ising interaction and next-nearest-neighbor XY interaction). Then, instead of the CDW phase obtained for the $t_2 - V_1$ model, we get a spin density wave (SDW) for the spin model of Eq. (2); the spin-model system will transit from a superfluid phase to a homogeneously coexisting SDW-superfluid phase.

Next, we will map our $t_2 - V_1$ model onto the following two-species model involving HCBs a in one sublattice and HCBs b in the other sublattice:

$$H = -t_2 \sum_{\langle i_a, j_a \rangle} \left(a^\dagger_{i_a} a_{j_a} + \text{H.c.} \right) - t_2 \sum_{\langle i_b, j_b \rangle} \left(b^\dagger_{i_b} b_{j_b} + \text{H.c.} \right) + V_1 \sum_{\langle i_a, j_b \rangle} n^a_{i_a} n^b_{j_b} - \mu \sum_{i_a, i_b} \left(n^a_{i_a} + n^b_{i_b} \right), \tag{15}$$

where $a_{i_a}(b_{i_b})$ denotes the destruction operator of HCB a (b) at site i_a (i_b), with the number operator being expressed as $n^a_{i_a} = a^\dagger_{i_a} a_{i_a}$ ($n^b_{i_b} = b^\dagger_{i_b} b_{i_b}$); the sum $\sum_{\langle i_a, j_a \rangle}$ ($\sum_{\langle i_b, j_b \rangle}$) runs over

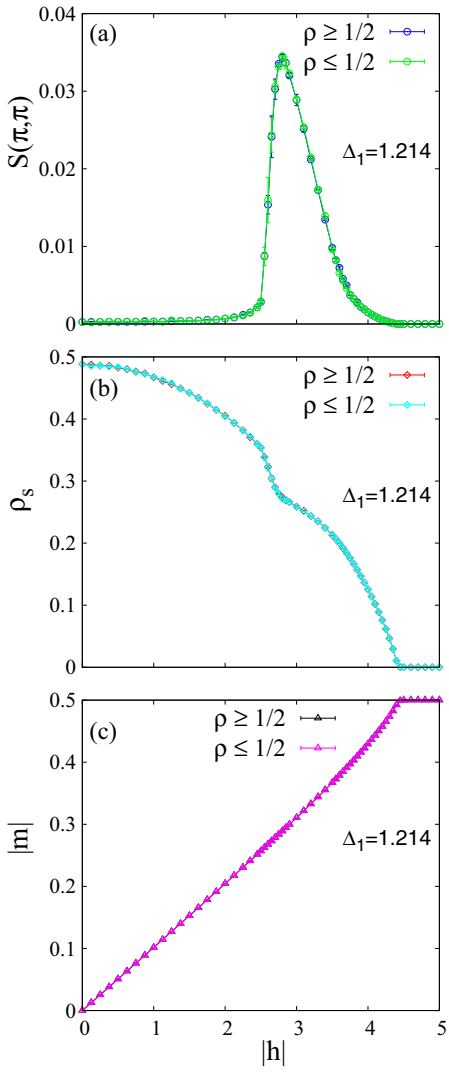

FIG. 10. Comparison of above-half-filling and below-half-filling plots of the order parameters $S(\pi, \pi)$, ρ_s and $|m|$ as a function of the magnetic field $|h|$, on a 32×32 lattice, for anisotropy $\Delta_1 = 1.214$. Magnetic field $h \geqslant 0$ and magnetization $m \geqslant 0$ ($h \leqslant 0$ and $m \leqslant 0$) correspond to $\rho \geqslant 1/2$ ($\rho \leqslant 1/2$).

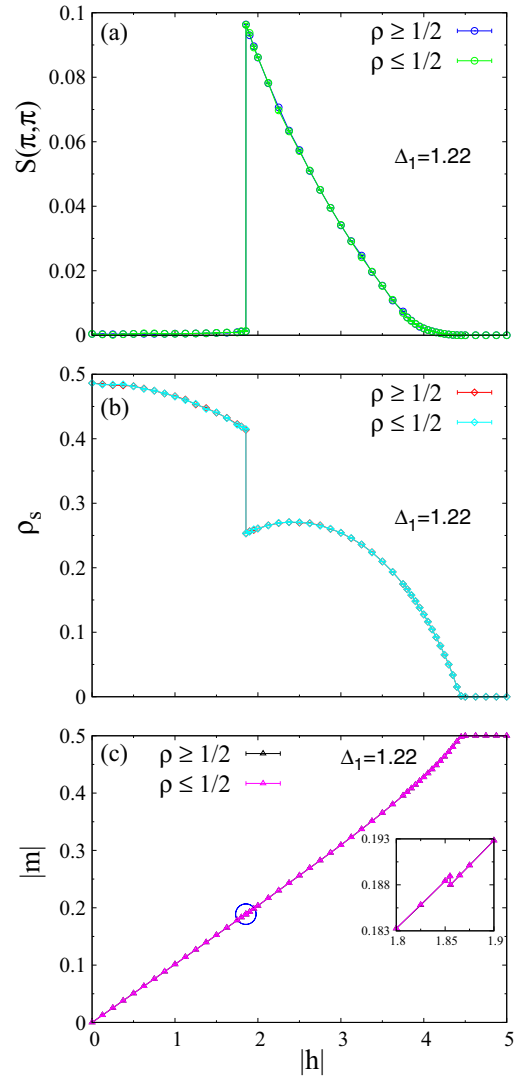

FIG. 11. Comparison of above-half-filling and below-half-filling plots of $S(\pi, \pi)$, ρ_s and $|m|$ as a function of the magnetic field $|h|$, on a 32×32 lattice, for anisotropy $\Delta_1 = 1.22$. $h \geqslant 0$ and $m \geqslant 0$ ($h \leqslant 0$ and $m \leqslant 0$) correspond to $\rho \geqslant 1/2$ ($\rho \leqslant 1/2$). The inset in (c) represents the magnified version of the region enclosed by the blue circle.

all distinct pairs of first neighboring sites i_a and j_a (i_b and j_b) in the sublattice containing HCBs a (b) and the sum $\sum_{\langle i_a, j_b\rangle}$ runs over all distinct pairs of nearest-neighboring sites i_a and j_b belonging to the two different sublattices; μ is the chemical potential that controls the total density of the two species. Then, in the above model given by Eq. (15), the system undergoes a transition from a superfluid to a phase with homogeneously coexisting superfluid and polarized state with polarization given by $|\sum_{i_a} n^a_{i_a} - \sum_{i_b} n^b_{i_b}|/(\sum_{i_a} n^a_{i_a} + \sum_{i_b} n^b_{i_b})$. Lastly, we also would like to point out that the model in Eq. (15) and the two-species Hubbard model [given below by Eq. (16)] are similar in terms of the kinetic term but different in terms of the interaction

$$H = -t \sum_{\langle i,j\rangle} (a_i^\dagger a_j + \text{H.c.}) - t \sum_{\langle i,j\rangle} (b_i^\dagger b_j + \text{H.c.}) + U_{ab} \sum_i n_i^a n_i^b - \mu \sum_i \left(n_i^a + n_i^b\right), \tag{16}$$

where a and b are two HCB species, the sum $\sum_{\langle i,j\rangle}$ runs over all distinct pairs of nearest-neighboring sites i and j, and $n_i^a = a_i^\dagger a_i$ ($n_i^b = b_i^\dagger b_i$). In the above model, given by Eq. (16), when the polarization $|\sum_i n_i^a - \sum_i n_i^b|/(\sum_i n_i^a + \sum_i n_i^b)$ attains its maximum value, we get a maximally polarized Nagaoka-like state [48] of the Hubbard model.

IV. SUMMARY

To summarize briefly, the present work deals with the $t_2 - V_1$ model which turns out to be the minimum model exhibiting checkerboard supersolidity for HCBs in a square lattice. This model has a well defined physical origin that goes back to dominant-particle-transport mechanism of double hopping realized in a system with cooperative normal mode at strong electron-phonon interaction. Alternately, it can always be realized in an optical lattice platform using cold atoms. The fascinating feature of this model is its rich ground state phase diagram characterized by various exotic phases and unusual quantum phase transitions. It shows a tricritical point, at an optimum strength V_1/t_2, that separates mixed-order and continuous transitions involving (π, π)-checkerboard orders. Importantly, the system displays extreme Thouless effect close to half filling.

ACKNOWLEDGMENTS

Authors thank Pinaki Sengupta and Deepak Dhar for valuable comments and suggestions on the work. Though all the numerics is done using the computational cluster at SINP, India, the final communication of the work occurred after AG joined Ben-Gurion University, Israel, under the funding and support of the Israel Innovation Authority, under the Kamin program as part of the QuantERA project InterPol. S.K. acknowledges the hospitality of SINP while part of this work was in progress.

APPENDIX: DEMONSTRATION OF ELECTRON-HOLE SYMMETRY

Here we demonstrate electron-hole symmetry by showing selectively that the order-parameter plots, at various values of magnetization m or magnetic field h, are identical for above and below half filling. In all the plots, $h \geqslant 0$ and $m \geqslant 0$ ($h \leqslant 0$ and $m \leqslant 0$) correspond to $\rho \geqslant 1/2$ ($\rho \leqslant 1/2$). In Figs. 8 and 9, we show that at any absolute value of the magnetization, both above half filling and below half filling, the same values are obtained for the order parameters $S(\pi, \pi)$ and ρ_s at anisotropies $\Delta_1 = 1.214$ and $\Delta_1 = 1.22$. Similarly, in Figs. 10 and 11, we make obvious that at any absolute value of the magnetic field, the plots for the order parameters $S(\pi, \pi)$, ρ_s and $|m|$ at above half filling overlap with those at below half filling when $\Delta_1 = 1.214$ and $\Delta_1 = 1.22$.

[1] I. Bloch, J. Dalibard, and W. Zwerger, Rev. Mod. Phys. **80**, 885 (2008).
[2] R. Landig, L. Hruby, N. Dogra, M. Landini, R. Mottl, T. Donner, and T. Esslinger, Nature (London) **532**, 476 (2016).
[3] R. Mottl, F. Brennecke, K. Baumann, R. Landig, T. Donner, and T. Esslinger, Science **336**, 1570 (2012).
[4] H. Ritsch, P. Domokos, F. Brennecke, and T. Esslinger, Rev. Mod. Phys. **85**, 553 (2013).
[5] D. Jaksch, C. Bruder, J. I. Cirac, C. W. Gardiner, and P. Zoller, Phys. Rev. Lett. **81**, 3108 (1998).
[6] G. G. Batrouni and R. T. Scalettar, Phys. Rev. Lett. **84**, 1599 (2000).
[7] F. Hébert, G. G. Batrouni, R. T. Scalettar, G. Schmid, M. Troyer, and A. Dorneich, Phys. Rev. B **65**, 014513 (2001).
[8] L. Dang, M. Boninsegni and L. Pollet, Phys. Rev. B **78**, 132512 (2008).
[9] B. Capogrosso-Sansone, C. Trefzger, M. Lewenstein, P. Zoller, and G. Pupillo, Phys. Rev. Lett. **104**, 125301 (2010).
[10] Y.-C. Chen, R. G. Melko, S. Wessel, and Y.-J. Kao, Phys. Rev. B **77**, 014524 (2008).
[11] P. Sengupta, L. P. Pryadko, F. Alet, M. Troyer, and G. Schmid, Phys. Rev. Lett. **94**, 207202 (2005).
[12] G. Schmid and M. Troyer, Phys. Rev. Lett. **93**, 067003 (2004).
[13] S. Kar and S. Yarlagadda, Ann. Phys. **375**, 322 (2016).
[14] S. Datta and S. Yarlagadda, Solid State Commun. **150**, 2040 (2010).
[15] X. Huo, Y.-Y. Cui, D. Wang, and J.-P. Lv, Phys. Rev. A **95**, 023613 (2017).
[16] A. M. Gabovich, A. I. Voitenko, and M. Ausloos, Phys. Rep. **367**, 583 (2002).
[17] S. H. Blanton, R. T. Collins, K. H. Kelleher, L. D. Rotter, Z. Schlesinger, D. G. Hinks, and Y. Zheng, Phys. Rev. B **47**, 996 (1993).
[18] R. L. Withers and J. A. Wilson, J. Phys. C **19**, 4809 (1986).
[19] J. Merino and R. H. McKenzie, Phys. Rev. Lett. **87**, 237002 (2001).
[20] W. W. Fuller, P. M. Chaikin, and N. P. Ong, Phys. Rev. B **24**, 1333 (1981).
[21] A. Rusydi, W. Ku, B. Schulz, R. Rauer, I. Mahns, D. Qi, X. Gao, A. T. S. Wee, P. Abbamonte, H. Eisaki, Y. Fujimaki, S. Uchida, and M. Rübhausen, Phys. Rev. Lett. **105**, 026402 (2010).

[22] P. Abbamonte, G. Blumberg, A. Rusydi, A. Gozar, P. G. Evans, T. Siegrist, L. Venema, H. Eisaki, E. D. Isaacs, and G. A. Sawatzky, Nature (London) **431**, 1078 (2004).
[23] G. G. Batrouni, F. Hébert, and R. T. Scalettar, Phys. Rev. Lett. **97**, 087209 (2006).
[24] S. Wessel, Phys. Rev. B **75**, 174301 (2007).
[25] S. Wessel and M. Troyer, Phys. Rev. Lett. **95**, 127205 (2005).
[26] M. Boninsegni and N. Prokof'ev, Phys. Rev. Lett. **95**, 237204 (2005).
[27] A. Lanzara, N. L. Saini, M. Brunelli, F. Natali, A. Bianconi, P. G. Radaelli, and S.-W. Cheong, Phys. Rev. Lett. **81**, 878 (1998).
[28] A. Damascelli, Z. Hussain, and Z. X. Shen, Rev. Mod. Phys. **75**, 473 (2003).
[29] A. Taraphder, R. Pandit, H. R. Krishnamurthy, and T. V. Ramakrishnan, Int. J. Mod. Phys. B **10**, 863 (1996).
[30] R. Pankaj and S. Yarlagadda, Phys. Rev. B **86**, 035453 (2012).
[31] A. Ghosh and S. Yarlagadda, Phys. Rev. B **90**, 045140 (2014).
[32] A. Ghosh and S. Yarlagadda, Phys. Rev. B **96**, 125108 (2017).
[33] D. J. Thouless, Phys. Rev. **187**, 732 (1969).
[34] D. J. Gross, I. Kanter, and H. Sompolinsky, Phys. Rev. Lett. **55**, 304 (1985).
[35] R. Blossey and J. O. Indekeu, Phys. Rev. E **52**, 1223 (1995).
[36] Y. Kafri, D. Mukamel, and L. Peliti, Phys. Rev. Lett. **85**, 4988 (2000).
[37] J. M. Schwarz, A. J. Liu, and L. Q. Chayes, Europhys. Lett. **73**, 560 (2006).
[38] C. Toninelli, G. Biroli, and D. S. Fisher, Phys. Rev. Lett. **96**, 035702 (2006).
[39] A. Bar and D. Mukamel, Phys. Rev. Lett. **112**, 015701 (2014).
[40] A. Bar and D. Mukamel, J. Stat. Mech. (2014) P11001.
[41] K. E. Bassler, D. Dhar, and R. K. P. Zia, J. Stat. Mech. (2015) P07013.
[42] A. W. Sandvik, Phys. Rev. B **56**, 11678 (1997).
[43] A. W. Sandvik, in *Lectures on the Physics of Strongly Correlated Systems XIV: Fourteenth Training Course in the Physics of Strongly Correlated Systems*, edited by A. Avella and F. Mancini, AIP Conf. Proc. No. 1297 (AIP, New York, 2010), p. 135.
[44] O. F. Syljuåsen and A. W. Sandvik, Phys. Rev. E **66**, 046701 (2002).
[45] O. F. Syljuåsen, Phys. Rev. E **67**, 046701 (2003).
[46] M. Boninsegni and N. V. Prokof'ev, Rev. Mod. Phys. **84**, 759 (2012).
[47] G. G. Batrouni, R. T. Scalettar, G. T. Zimanyi, and A. P. Kampf, Phys. Rev. Lett. **74**, 2527 (1995).
[48] Th. Hanisch and E. Müller-Hartmann, Ann. Phys. **505**, 381 (1993).